Graviton production through photon-quark scattering at the LHC

İ. Şahin,[1,*] M. Köksal,[2,†] S. C. İnan,[2,‡] A. A. Billur,[2,§]

B. Şahin,[1,¶] P. Tektaş,[1] E. Alıcı,[3] and R. Yıldırım[2]

[1]*Department of Physics, Faculty of Sciences,*

Ankara University, 06100 Tandogan, Ankara, Turkey

[2]*Department of Physics, Cumhuriyet University, 58140 Sivas, Turkey*

[3]*Department of Physics, Bulent Ecevit University, 67100 Zonguldak, Turkey*

arXiv:1409.1796v3 [hep-ph] 16 Jan 2015

Abstract

We have investigated real graviton emission in the ADD and RS model of extra dimensions through the photoproduction process $pp \to p\gamma p \to pGqX$ at the LHC. We have considered all contributions from the subprocesses $\gamma q \to Gq$, where $q = u, d, c, s, b, \bar{u}, \bar{d}, \bar{c}, \bar{s}, \bar{b}$ quark. The constraints on model parameters of the ADD and RS model of extra dimensions have been calculated. During numerical calculations we have taken account of 3, 4, 5 and 6 large extra dimensional scenarios. The constraints on RS model parameters have been calculated by considering $G \to \gamma\gamma, e\bar{e}, \mu\bar{\mu}$ decay channels of the graviton.

*inancsahin@ankara.edu.tr

†mkoksal@cumhuriyet.edu.tr

‡sceminan@cumhuriyet.edu.tr

§abillur@cumhuriyet.edu.tr

¶banusahin@ankara.edu.tr

I. INTRODUCTION

One of the leading aims of the Large Hadron Collider (LHC) is to discover new physics beyond the Standard Model. In this respect, extra dimensional models in particle physics have been drawing attention for the past fifteen years. These models offer a solution to the hierarchy problem, and provide possible candidates for dark matter. Phenomenology of extra dimensional models at the LHC has been widely studied in the literature as a possible new physics candidate. These phenomenological studies generally involve usual proton-proton deep inelastic scattering (DIS) processes where both of the colliding protons dissociate into partons. Subprocesses of quark-quark, gluon-gluon, and quark-gluon scattering have been probed in detail. On the other hand, exclusive production and semi-elastic processes have been much less studied in the literature. In an exclusive production process both of the incoming protons remains intact. They do not dissociate into partons. However in a semi-elastic scattering process, one of the incoming proton dissociate into partons but the other proton remains intact [1, 2]. The exclusive and semi-elastic proton processes are characterized by the interchange of photons or pomerons. The former generally give larger cross sections since the survival probability for processes involving a photon interchange is larger than that for a pomeron interchange. The exclusive and semi-elastic photon-mediated processes are sometimes called two-photon and photoproduction processes respectively. Phenomenology of extra dimensions has not been studied comprehensively in these types of processes. Extra dimensional models have been examined via the following two-photon processes: $pp \to p\gamma\gamma p \to p\ell\bar{\ell}p$ [3], $pp \to p\gamma\gamma p \to p\gamma\gamma p$ [4, 5], $pp \to p\gamma\gamma p \to p\Phi p$ [6], $pp \to p\gamma\gamma p \to pt\bar{t}p$ [7] and $pp \to p\gamma\gamma p \to pGp$ [8]. As far as we know, except for our recent paper [9] phenomenology of extra dimensional models has not been studied and model parameters have not been constrained in any photoproduction process at the LHC. In our recent paper we have analyzed the virtual effects of Kaluza-Klein (KK) gravitons in $pp \to p\gamma p \to p\gamma qX$. In this paper we will investigate real KK graviton emission through the photoproduction process $pp \to p\gamma p \to pGqX$ (Fig.1). $pp \to p\gamma p \to pGqX$ consists of the

following subprocesses:

$$\begin{aligned}
&\text{(i)}\ \ \gamma u \to G u && \text{(vi)}\ \ \gamma \bar{u} \to G \bar{u} \\
&\text{(ii)}\ \ \gamma d \to G d && \text{(vii)}\ \ \gamma \bar{d} \to G \bar{d} \\
&\text{(iii)}\ \ \gamma c \to G c && \text{(viii)}\ \ \gamma \bar{c} \to G \bar{c} \\
&\text{(iv)}\ \ \gamma s \to G s && \text{(ix)}\ \ \gamma \bar{s} \to G \bar{s} \\
&\text{(v)}\ \ \gamma b \to G b && \text{(x)}\ \ \gamma \bar{b} \to G \bar{b}
\end{aligned} \tag{1}$$

Therefore, in order to obtain the cross section for the main process $pp \to p\gamma p \to pGqX$ we have to consider all contributions coming from subprocesses in (1).

In a photoproduction process emitted photons from the proton ought to carry a small amount of virtuality. (Otherwise, proton dissociates after the emission.) Thus, the equivalent photon approximation (EPA) can be successfully applied to a photoproduction process. In EPA we employ the formalism of [10–12], and take account of the electromagnetic form factors of the proton. Hence, EPA formula that we have used is different from the pointlike electron or positron case.

Exclusive two-photon and photoproduction processes can be distinguished from fully inelastic processes by the virtue of the following experimental signatures: After the elastic emission of a photon, proton is scattered with a small angle and escapes detection from the central detectors. This causes a missing energy signature called *forward large-rapidity gap*, in the corresponding forward region of the central detector [1, 2, 13]. This technique was successfully used at the Fermilab Tevatron by the CDF Collaboration. Exclusive production of $\ell\bar{\ell}$, $\gamma\gamma$, jj and J/ψ were observed experimentally [14–18]. CMS Collaboration has also observed exclusive production of $\ell\bar{\ell}$ and W^+W^- pairs using early LHC data at $\sqrt{s}$=7 TeV [19–21]. Another experimental signature can be implemented by forward proton tagging. There are some proposals that aim to equip ATLAS and CMS central detectors with very forward detectors (VFD) which can detect intact scattered protons with a large pseudo-rapidity. Forward proton tagging in VFD supports forward large-rapidity gap signatures obtained from the central detectors. Operation of VFD in conjunction with central detectors with a precise timing, can efficiently reduce backgrounds from pile-up events [22–25]. It is argued that pile-up background grows rapidly with luminosity and becomes important for high luminosity runs at the LHC.

Apart from extra dimensions other new physics scenarios have also been studied via two-photon and photoproduction processes at the LHC. Phenomenological studies involve new physics scenarios such as supersymmetry, unparticles, technicolor, magnetic monopoles and model independent analysis of anomalous interactions [26–58].

II. EXTRA DIMENSIONAL MODELS AND CROSS SECTIONS

In this paper we will focus on two different extra dimensional models, namely, Arkani-Hamed, Dimopoulos and Dvali (ADD) model of large extra dimensions [59–61] and Randall and Sundrum (RS) model of warped extra dimensions [62]. The ADD model assumes a $(4+\delta)$-dimensional spacetime where δ represents the number of extra spatial dimensions. Extra dimensions are flat and compactified in a volume V_δ. For instance, we can consider a toroidal compactification of volume $V_\delta = (2\pi R)^\delta$. Here, R represents the radii of extra dimensions. In the ADD model, extra dimensions can be as large as approximately 0.1 mm. For this reason ADD model is sometimes called the large extra dimensional model. In principle, the number of extra dimensions can be $\delta \geq 1$. But astronomical observations on Newton's gravitation law rule out $\delta = 1$ case. There are also constraints from table top experiments and astrophysical observations. These constraints are stringent for $\delta = 2$. Hence, we will consider the case in which $\delta \geq 3$. The ADD model solves the hierarchy problem by introducing a new mass scale M_D called the fundamental scale which is at the order of electroweak scale. M_D is the mass scale of the $(4+\delta)$-dimensional theory. Thus, it is argued by the model that the true mass scale of the theory is M_D, not the Planck scale M_{Pl}. On the other hand, an observer confined in a 4-dimensional spacetime measures its value as M_{Pl}.

The original version of the RS model assumes the existence of only one extra spatial dimension and two 3-branes (4-dimensional spacetimes) located at boundaries of the extra dimensional coordinate y. The metric is given by [62]

$$ds^2 = e^{-2k|y|}\eta_{\mu\nu}dx^\mu dx^\nu - dy^2, \tag{2}$$

where k represents a constant of the order of the Planck scale. The metric (2) describes a 5-dimensional anti-de Sitter space with a cosmological constant Λ. Extra dimensional coordinate y can be parametrized by an angular coordinate ϕ via $y = r_c\phi$. Here, r_c represents

the compactification radius of the extra dimension. The angular coordinate varies in the range $0 \leq |\phi| \leq \pi$. It is assumed that we are living in the 3-brane located at the boundary point $\phi = \pi$. It is deduced from the model that any mass scale m observed in $\phi = \pi$ brane is generated from the fundamental mass scale m_0 which is at the order of M_{Pl}. The relation between these two scales is given by: $m = m_0 e^{-kr_c\pi}$. Thus, the hierarchy problem is eliminated.

Both the ADD and RS model of extra dimensions involve massive gravitons and gravitational scalars which are possible dark matter candidates. On the other hand, mass scales for these new particles are very different in the ADD and RS models. This leads to different phenomenologies. In the ADD model of extra dimensions, mass difference between consecutive graviton excited states is given approximately by the formula [63, 64]:

$$\Delta m \approx \frac{M_D^{\frac{2+\delta}{\delta}}}{\bar{M_{Pl}}^{\frac{2}{\delta}}} \tag{3}$$

We see from this formula that mass splitting is quite narrow. For instance, if we choose $M_D = 1$ TeV and $\delta = 4$ then $\Delta m \approx 50$ KeV. Therefore, at collider energies KK graviton production processes involve a summation over huge number of graviton final states. This summation can be approximated to an integral and the cross section for the inclusive production process can be written as [63]

$$\sigma = \int\int \left(\frac{d^2\sigma}{dmdt}\right) dmdt \tag{4}$$

$$\frac{d^2\sigma}{dmdt} = \frac{2\pi^{\delta/2}}{\Gamma(\delta/2)} \frac{\bar{M_{Pl}}^2}{M_D{}^{2+\delta}} m^{\delta-1} \frac{d\sigma_m}{dt} \tag{5}$$

where $\frac{d\sigma_m}{dt}$ is the cross section for producing a single KK graviton state of mass m. The differential cross section $\frac{d\sigma_m}{dt}$ can be obtained in conventional way from the scattering amplitude. Since the masses of KK states are integrated, total cross section in Eq. (4) depends on two model parameters M_D and δ.

In the RS model case, the spectrum of KK graviton masses is given by [65]

$$m_n = x_n k e^{-kr_c\pi} = x_n \beta \Lambda_\pi, \quad \beta = k/\bar{M}_{Pl} \tag{6}$$

where x_n are the roots of the Bessel function J_1, i.e., $J_1(x_n) = 0$. We can deduce from this formula that mass splitting between consecutive KK graviton states is considerably large,

$\sim \mathcal{O}(TeV)$. Hence it is assumed that only the first KK graviton state can be observed. We will represent the mass of this first KK graviton state by m_G. Masses of other KK states are proportional to m_G: $m_n = \frac{x_n}{x_1} m_G$. In the RS model we have two independent model parameters. We prefer to choose m_G and β as independent parameters.

The process $\gamma q \to Gq$ is represented by the Feynman diagrams in Fig.2. We do not give the Feynman rules for KK gravitons. One can find the Feynman rules in Refs. [63, 64]. Analytical expressions for the scattering amplitude are given in the Appendix. As we have mentioned in the introduction we consider all possible initial quark flavors. Thus, in order to obtain the total cross section for the process $pp \to p\gamma p \to pGqX$ we integrate the subprocess cross sections over the photon and quark distributions and sum all contributions from different subprocesses:

$$\sigma\left(pp \to p\gamma p \to pGqX\right) = \sum_q \int_{\xi_{min}}^{\xi_{max}} dx_1 \int_0^1 dx_2 \left(\frac{dN_\gamma}{dx_1}\right)\left(\frac{dN_q}{dx_2}\right) \sigma(\gamma q \to Gq) \qquad (7)$$

Here, x_1 represents the energy ratio between the equivalent photon and incoming proton and x_2 is the fraction of the proton's momentum carried by the struck quark. $\frac{dN_\gamma}{dx_1}$ and $\frac{dN_q}{dx_2}$ are the equivalent photon and quark distribution functions. The analytical expression for $\frac{dN_\gamma}{dx_1}$ can be found in the literature, for example in [9–12] or [32]. $\frac{dN_q}{dx_2}$ can be evaluated numerically. In this paper we have used parton distribution functions of Martin *et al.* [66].

III. NUMERICAL RESULTS

During numerical calculations we assume the existence of VFD proposed by Refs. [22, 32, 67, 68]. In Refs. [22, 67], it was proposed to locate VFD at 220 m and 420 m distances away from the ATLAS interaction point. These detectors can detect forward protons within the acceptance region $0.0015 < \xi < 0.15$. Here, $\xi \equiv (|\vec{p}| - |\vec{p}\,'|)/|\vec{p}|$ where $\vec{p}$ represents the initial proton's momentum and $\vec{p}\,'$ represents forward proton's momentum after scattering. According to another scenario VFD can detect forward protons within $0.0015 < \xi < 0.5$ [32, 68]. This scenario is based on VFD located at 420 m distance from the CMS interaction point and TOTEM detectors at 147 m and 220 m.

For all numerical results presented in this paper, the center-of-mass energy of the proton-proton system is taken to be $\sqrt{s} = 14$ TeV and the virtuality of the DIS is taken to be $Q^2 = (5M_Z)^2 \approx (456\ GeV)^2$. Here, M_Z is the mass of the Z boson and it represents only

a scale which is roughly at the order of Standard Model energies. This virtuality value is reasonable since the average value for the square of the momentum transferred to the proton is approximately at that order. Moreover, at high energies parton distribution functions do not depend significantly on virtuality. Thus, it is reasonable to use a fix virtuality value for the DIS.

In Fig.3 and Fig.4 we present ADD model cross section of the process $pp \to p\gamma p \to pGqX$ as a function of the fundamental scale M_D for VFD acceptances of $0.0015 < \xi < 0.5$ and $0.0015 < \xi < 0.15$ respectively. We consider the cases in which the number of extra spatial dimensions are $\delta = 3, 4, 5, 6$. We see from these figures that cross section decreases with increasing δ. Moreover, cross sections for different number of extra dimensions significantly deviate from each other for large M_D values. These behaviors are obvious from differential cross section formula in Eq. (5). As we have discussed in the previous section, ADD graviton final states consist of huge number of KK states arranged densely with increasing mass. This sequence of states is sometimes called a KK tower. A KK tower is not detected directly in the detectors. Instead, its presence is inferred from missing energy signal. Missing signal for a KK tower exhibits a peculiarity which is very different compared with any other new physics processes [63]. The peculiarity originates from continuous mass distribution of graviton states in a KK tower. Different from other new physics or Standard Model processes, we do not have a fix final state mass. But the cross section is integrated over the mass of final state gravitons (see Eq. (4)). Thus, the momentum carried by a KK tower can take values which are kinematically forbidden in the fix mass case. This peculiar behavior is reflected in missing transverse momentum and invariant mass distributions and useful when we want to discern graviton production from other new physics processes and Standard Model backgrounds. In Fig.5-Fig.8 we present missing p_T (p_T of the KK tower) dependence of the cross section of the process $pp \to p\gamma p \to pGqX$ for various number of extra dimensions δ. In these figures VFD acceptance is taken to be $0.0015 < \xi < 0.5$ and M_D=5 TeV. p_T distributions for $0.0015 < \xi < 0.15$ case exhibit similar behaviors.

The main background to our process is $pp \to p\gamma p \to p\nu\bar{\nu}qX$. This background process consists of the following subprocesses: $\gamma q \to \nu\bar{\nu}q$ where $q = u, d, c, s, b, \bar{u}, \bar{d}, \bar{c}, \bar{s}, \bar{b}$ quark and $\nu = \nu_e, \nu_\mu, \nu_\tau$. Since the final state neutrinos are not detected in the detectors they may generate a missing signal similar to the one coming from graviton production. But as we have discussed before, the missing signal associated with final state neutrino pair exhibits

a different behavior and can be discerned from the missing signal associated with a KK tower. In Fig.9 and Fig.10 we plot missing transverse momentum and missing invariant mass dependence of the cross section both for our process and the Standard Model background. In these figures cross sections have been calculated by considering all contributions from possible subprocesses. As can be seen from Fig.9 and Fig.10 signal and background cross sections are well separated from each other. We observe from Fig.9 that differential cross section for the background rapidly decreases as p_T increases and it is suppressed for $p_T > 300$ GeV. Graviton production cross section also decreases with increasing p_T. However, the decrease is approximately linear up to $p_T \approx 3000$ GeV (not shown in the figure). The missing invariant mass $M_{Inv} = \sqrt{E_{miss}^2 - |\vec{P}_{miss}|^2}$ dependence of the cross section exhibit similar behaviors. We see from Fig.10 that background cross section rapidly decreases after the peak point around $M_{Inv} \approx M_Z$ and it is suppressed for $M_{Inv} > 600$ GeV. On the other hand, graviton production cross section does not change considerably for 600 GeV $< M_{Inv} <$ 5000 GeV (not shown in the figure). Hence, the background can be discerned from the ADD signal and can be eliminated by imposing a cut on the missing invariant mass or missing transverse momentum.

In the RS model, we aim to observe first KK graviton state with mass m_G. Similar to techniques used to detect a massive particle such as W, Z boson or top quark, an RS graviton can be detected from its decay products. Angular distribution of the RS graviton for the process $pp \to p\gamma p \to pGqX$ is given in Fig.11. We consider VFD acceptance of $0.0015 < \xi < 0.5$ but we expect a similar behavior for $0.0015 < \xi < 0.15$ case. In the figure, we show both the the cross section including the sum of all contributions from subprocesses in (1) and cross sections including individual contributions from each subprocess.

We have obtained 95% confidence level (CL) bounds on the model parameters of the ADD and RS models. Since the Standard Model contribution to the process is absent and the backgrounds can be eliminated it is appropriate to employ a statistical analysis using a Poisson distribution. In the ADD model case, the expected number of events is calculated from the formula: $N = S \times E \times \sigma(pp \to p\gamma p \to pGqX) \times L_{int}$. In this formula, S represents the survival probability factor, E represents the jet reconstruction efficiency and L_{int} represents the integrated luminosity. We take into account a survival probability factor of $S = 0.7$ and jet reconstruction efficiency of $E = 0.6$. We also place a pseudorapidity cut of $|\eta| < 2.5$ for final quarks and antiquarks from subprocesses in (1). In Tables I and

II we present 95% CL bounds on the fundamental scale for various values of L_{int} and δ without imposing a cut on the missing invariant mass or missing transverse momentum. In Tables III and IV we present similar bounds but in this case we impose a missing invariant mass cut of $M_{Inv} > 600$ GeV. As we have discussed, this cut effectively eliminates the background contribution. We observe from Tables I - IV that the effect of the cut on the sensitivity bounds is minor. The bounds on M_D are slightly spoiled. For instance, when we compare the bounds in Tables I and III we see that the percentage differences between bounds with and without a cut do not exceed 4%, 1%, 0.5% and 0.3% for $\delta = 3, 4, 5$ and 6 respectively. In the RS model, bounds are calculated in the plane of β versus m_G. Since an RS graviton can be detected from its decay products, the expected number of events is given by $N = S \times E \times \sigma(pp \to p\gamma p \to pGqX) \times L_{int} \times BR$, where BR represents the branching ratio for the graviton. We place a pseudorapidity cut of $|\eta| < 2.5$ for final quarks, antiquarks and also the graviton. The limits have been calculated by considering $G \to \gamma\gamma, e\bar{e}, \mu\bar{\mu}$ decay channels of the RS graviton with a total branching ratio of 8% [69]. In Fig.12 we present the excluded regions in the β versus m_G parameter plane for the above branching ratio value. The Standard Model processes $pp \to p\gamma p \to p\ (\gamma\gamma, e\bar{e}, \mu\bar{\mu})qX$ give rise to the same final states. Determination of an on-shell graviton with mass $\mathcal{O}(TeV)$ requires an invariant mass measurement of the final state charged lepton and photon pairs. Therefore, we should impose a cut of $M_{\gamma\gamma,e\bar{e},\mu\bar{\mu}} \approx m_G \approx \mathcal{O}(TeV)$ on the invariant mass of final leptons and photons. This cut reduces the effect of background processes drastically. To be precise, the sum of all Standard Model contributions, i.e., sum of the cross sections for the processes $pp \to p\gamma p \to p\ k\bar{k}qX$ where $k = \gamma, e, \mu$ and $q = u, d, c, s, b, \bar{u}, \bar{d}, \bar{c}, \bar{s}, \bar{b}$ quark, provides a huge cross section of 1.3×10^3 pb. But if we demand that the invariant mass of final state lepton and photon pairs are in the interval 990 GeV $< M_{\gamma\gamma,e\bar{e},\mu\bar{\mu}} <$ 1010 GeV, then the total Standard Model contribution becomes only 2.4×10^{-6} pb. Thus, the background contribution is reduced by approximately a factor of 10^9. The number of Standard Model events is smaller than 1 and therefore the background contributions can be ignored.

IV. CONCLUSIONS

Processes involving real graviton final states provide a direct signal for TeV-scale gravity. In the ADD model of extra dimensions, KK gravitons behave like non-interacting stable

particles and their presence are inferred from missing energy signal [63]. But as we have discussed in the previous section, missing signal associated with ADD gravitons exhibits a peculiar behavior which is very different compared with any other new physics models and Standard Model backgrounds. This peculiar behavior allows us to isolate signals coming from graviton production. In the RS model of extra dimensions, KK gravitons can be detected via their decay products. The angular distribution of its decay products can be used to determine the spin of the graviton [69]. In case a particle having a spin of 2 and a mass of $\mathcal{O}(TeV)$ is detected, this will be a distinctive signature for the model. Many new physics scenarios can be eliminated by means of this signature. As we have shown, invariant mass cut on the decay products of the graviton effectively eliminates the background contributions. Therefore, graviton production processes provide important clues for the models of TeV-scale gravity. These type of processes give us the opportunity to isolate and discern the model which is much more difficult for processes in which virtual effects of KK gravitons are considered.

Virtual effects of KK gravitons were examined in the following two-photon and photoproduction processes at the LHC: $pp \to p\gamma\gamma p \to p\ell\bar{\ell}p$ [3], $pp \to p\gamma\gamma p \to p\gamma\gamma p$ [4, 5], $pp \to p\gamma\gamma p \to pt\bar{t}p$ [7] and $pp \to p\gamma p \to p\gamma qX$ [9]. A comparison of our limits with the limits obtained in these processes is difficult in the case of the ADD model. It is because in these papers authors used the cutoff procedure of Giudice *et al.* [63] in the graviton propagator that the cross section depends only on the cutoff scale. It is independent of the number of extra dimensions δ. On the other hand, if we assume that the convention of Giudice *et al.* corresponds to $\delta = 4$ case [1] then our present limits on the fundamental scale are better than the limits obtained in two-photon processes [3–5, 7] but approximately at the same order with the limits of our recent paper [9]. When we compare our RS limits with the limits from processes mentioned above we see that our limits in the plane of β versus m_G are stronger than the limits obtained in [3, 7] but approximately at the same order with the limits of [4, 9]. To be precise, our limits for Atlas VFD scenario are little better but our limits for CMS-TOTEM VFD scenario are little worse than the corresponding limits obtained in [9]. In Ref. [4] only CMS-TOTEM VFD scenario was considered for the RS model case.

[1] Han *et al.* [64] employed a different cutoff procedure. According to the convention of Han *et al.* the summation of KK states in the propagator is approximated to an expression that depends on δ. Conventions of Han *et al.* and Giudice *et al.* coincide for $\delta = 4$.

Thus, a comparison for Atlas VFD scenario is impossible. Real graviton and radion final states were investigated in the following two-photon processes: $pp \to p\gamma\gamma p \to pGp$ [8] and $pp \to p\gamma\gamma p \to p\Phi p$ [6]. In Ref. [6] authors considered only the RS model case and it seems they did not obtain the limits on RS model parameters. In Ref. [8] the full decay channel of the RS graviton is considered i.e., $BR = 100\%$. Hence, it is very difficult to compare our RS limits with the corresponding limits of [8]. On the other hand, our ADD limits are a percentage from 250% to 500% better than the limits obtained in [8] depending on the luminosity, VFD acceptance and δ.

The current best experimental bounds on the ADD and RS model parameters are provided by the ATLAS and CMS collaborations at the CERN LHC [70–79]. The most stringent bounds on the ADD model parameters to date have been obtained in proton-proton collisions with a center-of-mass energy of $\sqrt{s} = 8$ TeV and an integrated luminosity of approximately $L_{int} = 20 fb^{-1}$ [77–79]. When we compare our ADD limits with the most stringent experimental limits obtained at the LHC we see that our limits for a VFD acceptance of $0.0015 < \xi < 0.5$ and an integrated luminosity of $L_{int} = 200 fb^{-1}$ are a percentage from 125% to 150% better than these experimental bounds depending on the value of δ. Experimental bounds on the RS model parameters have been obtained by considering graviton resonances decaying to e^-e^+, $\mu^-\mu^+$ and $\gamma\gamma$ final states [73–75]. These experimental bounds are stronger than the bounds that we have obtained. Our RS limits for similar final states (Fig.12) are approximately 50% worse than these experimental limits. In conclusion, the photoproduction process $pp \to p\gamma p \to pGqX$ at the LHC possesses a remarkable potential in searching for the extra dimensional scenario proposed by the ADD model. On the contrary, its potential is low in probing warped extra dimensional model of RS. Nevertheless, $pp \to p\gamma p \to pGqX$ process can also be used in combination with other processes in order to verify the universality feature of the graviton's coupling.

Acknowledgments

This work has been supported by the Scientific and Technological Research Council of Turkey (TÜBİTAK) in the framework of the project no: 112T085.

Appendix: Analytical expressions for the scattering amplitude

In the ADD model of extra dimensions the polarization summed amplitude square for the subprocess $\gamma q \to Gq$ is given by

$$|M|^2 = |M_1 + M_2 + M_3 + M_4|^2 \tag{A.1}$$

$$|M_1|^2 = -\frac{(qg_e)^2}{4\bar{M_{Pl}}^2}\frac{[40(m^4 - (s-t+u)m^2 + su)]}{3m^2} \tag{A.2}$$

$$\begin{aligned}|M_2|^2 = \frac{(qg_e)^2}{3t^2m^4\bar{M_{Pl}}^2} \quad & [-6m^{10} + 12tm^8 + 6((s+u)^2 - 2t^2)m^6 - 2t(6s^2 + ts - 6t^2 + \\ & 6u^2 + tu)m^4 + 2t^2(4s^2 + (t-4u)s - (3t-4u)(t+u))m^2 - \\ & 2t^3(s^2+u^2)]\end{aligned} \tag{A.3}$$

$$M_1^\dagger M_2 + M_2^\dagger M_1 = \frac{(qg_e)^2}{2t\bar{M_{Pl}}^2}\frac{[20(-2m^6 + (2s+t+2u)m^4 - 2t(s+u)m^2 + t^3 + 2stu)]}{3m^2} \tag{A.4}$$

$$\begin{aligned}|M_3|^2 = -\frac{(qg_e)^2}{48s^2m^4\bar{M_{Pl}}^2} \quad & [4s(2m^8 - (5s+t-4u)m^6 + 2(2s^2 - 4us + (t+u)(t+2u))m^4 \\ & -(s+3t-2u)(-s+t+u)^2m^2 + 2st(-s+t+u)^2)]\end{aligned} \tag{A.5}$$

$$\begin{aligned}M_1^\dagger M_3 + M_3^\dagger M_1 = -\frac{(qg_e)^2}{24sm^4\bar{M_{Pl}}^2} \quad & [32m^8 + (-60s + 4t - 68u)m^6 + 8(3s^2 + (t+7u)s + \\ & (t+u)(2t+5u))m^4 + 4(s^3 - 3(t-u)s^2 + 3(t-5u)(t+u)s \\ & -(t+u)^3)m^2 - 16s(s-t-u)u(t+u)]\end{aligned} \tag{A.6}$$

$$M_2^\dagger M_3 + M_3^\dagger M_2 = -\frac{(qg_e)^2}{12tsm^4{\bar{M}_{Pl}}^2} \quad [2((13s+3t-3u)m^8 - 2(12s^2+9ts-4t^2+4(s+t)u)m^6 + (12s^3+(6t+9u)s^2+t(25t+13u)s-(t-u)(13t^2+24ut + 3u^2))m^4 - (s^4+(u-6t)s^3+(11t^2+16ut-u^2)s^2 + (8t^3+15ut^2-2u^2t-u^3)s-2t(t-u)(t+u)(t+6u))m^2 - 2t(s-t-u)(u^3-t^2u+s^2(2t+3u)))] \tag{A.7}$$

$$|M_4|^2 = -\frac{(qg_e)^2}{48u^2m^4{\bar{M}_{Pl}}^2} \quad [4u(2m^8+(4s-t-5u)m^6+2(2s^2+3ts-4us+t^2+2u^2)m^4 + (2s-3t-u)(s+t-u)^2m^2+2t(s+t-u)^2u)] \tag{A.8}$$

$$M_1^\dagger M_4 + M_4^\dagger M_1 = -\frac{(qg_e)^2}{24um^4{\bar{M}_{Pl}}^2} \quad [4(8m^8+(-17s+t-15u)m^6+2(5s^2+7(t+u)s+2t^2 + 3u^2+tu)m^4+(-(s+t)^3-3(5s-t)u(s+t)+u^3 + 3(s-t)u^2)m^2+4s(s+t)(s+t-u)u)] \tag{A.9}$$

$$M_2^\dagger M_4 + M_4^\dagger M_2 = -\frac{(qg_e)^2}{12tum^4{\bar{M}_{Pl}}^2} \quad [2((-3s+3t+13u)m^8-2(-4t^2+9ut+12u^2 + 4s(t+u))m^6+(3s^3+21ts^2-11t^2s-13t^3+12u^3 + 3(3s+2t)u^2+t(13s+25t)u)m^4-(u^4+(s-6t)u^3 - (s^2-16ts-11t^2)u^2-(s^3+2ts^2-15t^2s-8t^3)u + 2(s-t)t(s+t)(6s+t))m^2+2t(s+t-u)(s^3-t^2s + 3u^2s+2tu^2))] \tag{A.10}$$

$$M_3^\dagger M_4 + M_4^\dagger M_3 = \frac{(qg_e)^2}{48sum^4{\bar{M}_{Pl}}^2} \quad [4(8tm^8+(s^2-15ts-2us-30t^2+u^2-15tu)m^6 + (-6s^3+6us^2+(26t^2+72ut+6u^2)s-12t^3-6u^3 + 26t^2u)m^4+(3s^4+(13t+8u)s^3-(13t^2+13tu+22u^2)s^2 - (13t^3+18ut^2+13u^2t-8u^3)s+(2t-3u)(t-u) (5t+u))m^2+2(s-t-u)(s+t-u)(s^3-us^2-(t+u)^2s + u^3-t^2u))] \tag{A.11}$$

where M_1, M_2, M_3 and M_4 are the amplitudes of the Feynman diagrams in Fig.2, s, t and u are Mandelstam parameters, m is the mass of the individual KK graviton, $g_e = \sqrt{4\pi\alpha}$, $q = -\frac{1}{3}$ for d,s and b quarks and $q = +\frac{2}{3}$ for u and c quarks. During amplitude calculations we neglect the mass of quarks. This is a good approximation at the LHC energies.

The amplitude square in the RS model can be obtained by the following replacement: $\bar{M}_{Pl} \to \sqrt{2}\,\Lambda_\pi$

[1] X. Rouby, Ph.D. thesis, Universite Catholique de Louvain [CERN-THESIS-2009-216 and CMS-TS-2009-004]

[2] N. Schul, Ph.D. thesis, Universite Catholique de Louvain [CERN-THESIS-2011-271 and CMS-TS-2011-030].

[3] S. Atağ, S. C. İnan and İ. Şahin, Phys. Rev. D **80**, 075009 (2009); arXiv:0904.2687 [hep-ph].

[4] S. Atağ, S. C. İnan and İ. Şahin, JHEP **09**, 042 (2010); arXiv:1005.4792 [hep-ph].

[5] H. Sun, Eur. Phys. J. C **74**, 2977 (2014) [arXiv:1406.3897 [hep-ph]].

[6] V. P. Goncalves and W. K. Sauter, Phys. Rev. D **82**, 056009 (2010) [arXiv:1007.5487 [hep-ph]].

[7] S. C. Inan and A. A. Billur, Phys. Rev. D **84**, 095002 (2011).

[8] S. C. Inan, Chin. Phys. Lett. **29**, 031301 (2012).

[9] İ. Şahin *et al.*, Phys. Rev. D **88**, 095016 (2013) [arXiv:1304.5737 [hep-ph]].

[10] V. M. Budnev, I. F. Ginzburg, G. V. Meledin and V. G. Serbo, Phys. Rep. **15**, 181 (1975).

[11] G. Baur *et al.*, Phys. Rep. **364**, 359 (2002).

[12] K. Piotrzkowski, Phys. Rev. D **63**, 071502 (2001) [hep-ex/0009065].

[13] M. Albrow *et al.* (CMS Collaboration), JINST **4**, P10001 (2009) [arXiv:0811.0120 [hep-ex]].

[14] A. Abulencia *et al.* (CDF Collaboration), Phys. Rev. Lett. **98**, 112001 (2007); arXiv:hep-ex/0611040.

[15] T. Aaltonen *et al.* (CDF Collaboration), Phys. Rev. Lett. **102**, 222002 (2009) [arXiv:0902.2816 [hep-ex]].

[16] T. Aaltonen *et al.* (CDF Collaboration), Phys. Rev. Lett. **108**, 081801 (2012) [arXiv:1112.0858 [hep-ex]].

[17] T. Aaltonen *et al.* (CDF Collaboration), Phys. Rev. D **77**, 052004 (2008) [arXiv:0712.0604 [hep-ex]].

[18] T. Aaltonen *et al.* (CDF Collaboration), Phys. Rev. Lett. **102**, 242001 (2009) [arXiv:0902.1271 [hep-ex]].

[19] S. Chatrchyan *et al.* (CMS Collaboration), JHEP **1201**, 052 (2012) [arXiv:1111.5536 [hep-ex]].

[20] S. Chatrchyan *et al.* (CMS Collaboration), JHEP **1211**, 080 (2012) [arXiv:1209.1666 [hep-ex]].

[21] S. Chatrchyan *et al.* (CMS Collaboration), JHEP **1307**, 116 (2013) [arXiv:1305.5596 [hep-ex]].

[22] M. G. Albrow *et al.* (FP420 R and D Collaboration), JINST **4**, T10001 (2009) [arXiv:0806.0302 [hep-ex]].

[23] M. Tasevsky, Nucl. Phys. Proc. Suppl. **179-180**, 187 (2008).

[24] M. G. Albrow, T. D. Coughlin and J. R. Forshaw, Prog. Part. Nucl. Phys. **65**, 149 (2010) [arXiv:1006.1289 [hep-ph]].

[25] M. Tasevsky, arXiv:1407.8332 [hep-ph].

[26] I. F. Ginzburg and A. Schiller, Phys. Rev. D **57**, 6599 (1998) [hep-ph/9802310].

[27] I. F. Ginzburg and A. Schiller, Phys. Rev. D **60**, 075016 (1999) [hep-ph/9903314].

[28] S. M. Lietti, A. A. Natale, C. G. Roldao and R. Rosenfeld, Phys. Lett. B **497**, 243 (2001); arXiv:hep-ph/0009289.

[29] V.A. Khoze, A.D. Martin and M.G. Ryskin, Eur. Phys. J. C **23**, 311 (2002); arXiv:hep-ph/0111078.

[30] N. Schul and K. Piotrzkowski, Nucl. Phys. B, Proc. Suppl., **179**, 289 (2008); arXiv:0806.1097 [hep-ph].

[31] T. Pierzchala and K. Piotrzkowski, Nucl. Phys. Proc. Suppl. **179-180**, 257 (2008); arXiv:0807.1121 [hep-ph].

[32] O. Kepka and C. Royon, Phys. Rev. D **78**, 073005 (2008); arXiv:0808.0322 [hep-ph].

[33] İ. Şahin and S. C. İnan, JHEP **09**, 069 (2009); arXiv:0907.3290 [hep-ph].

[34] T. Dougall and S. D. Wick, Eur. Phys. J. A **39**, 213 (2009) [arXiv:0706.1042 [hep-ph]].

[35] M. Chaichian, P. Hoyer, K. Huitu, V. A. Khoze and A. D. Pilkington, JHEP **0905**, 011 (2009) [arXiv:0901.3746 [hep-ph]].

[36] J. de Favereau de Jeneret, V. Lemaitre, Y. Liu, S. Ovyn, T. Pierzchala, K. Piotrzkowski, X. Rouby, N. Schul and M. Vander Donckt, arXiv:0908.2020 [hep-ph].

[37] E. Chapon, C. Royon and O. Kepka , Phys. Rev. D **81**, 074003 (2010); arXiv:0912.5161 [hep-ph].

[38] K. Piotrzkowski and N. Schul, AIP Conf. Proc. **1200**, 434 (2010) [arXiv:0910.0202 [hep-ph]].

[39] S. C. İnan, Phys. Rev. D **81**, 115002 (2010); arXiv:1005.3432 [hep-ph].

[40] S. Atağ and A. A. Billur, JHEP **11**, 060 (2010); arXiv:1005.2841 [hep-ph].

[41] İ. Şahin, and A. A. Billur, Phys. Rev. D **83**, 035011 (2011); arXiv:1101.4998 [hep-ph].

[42] İ. Şahin, and M. Koksal, JHEP **03**, 100 (2011); arXiv:1010.3434 [hep-ph].

[43] R. S. Gupta, Phys. Rev. D **85**, 014006 (2012) [arXiv:1111.3354 [hep-ph]].

[44] İ. Şahin, Phys. Rev. D **85**, 033002 (2012) [arXiv:1201.4364 [hep-ph]].

[45] L. N. Epele, H. Fanchiotti, C. A. G. Canal, V. A. Mitsou and V. Vento, Eur. Phys. J. Plus **127**, 60 (2012) [arXiv:1205.6120 [hep-ph]].

[46] B. Şahin and A. A. Billur, Phys. Rev. D **86**, 074026 (2012) [arXiv:1210.3235 [hep-ph]].

[47] İ. Şahin and B. Şahin, Phys. Rev. D **86**, 115001 (2012) [arXiv:1211.3100 [hep-ph]].

[48] A. A. Billur, Europhys. Lett. **101**, 21001 (2013).

[49] A. Senol, Phys. Rev. D **87**, 073003 (2013) [arXiv:1301.6914 [hep-ph]].

[50] M. Koksal and S. C. Inan, Adv. High Energy Phys. **2014**, 935840, (2014) [arXiv:1305.7096 [hep-ph]].

[51] H. Sun and C. X. Yue, Eur. Phys. J. C **74**, 2823 (2014) [arXiv:1401.0250 [hep-ph]].

[52] H. Sun, Nucl. Phys. B **886**, 691 (2014) [arXiv:1402.1817 [hep-ph]].

[53] A. Senol, A. T. Tasci, I. T. Cakir and O. Cakir, arXiv:1405.6050 [hep-ph].

[54] M. Koksal and S. C. Inan, Adv. High Energy Phys. **2014**, 315826 (2014) [arXiv:1403.2760 [hep-ph]].

[55] H. Sun, arXiv:1407.5356 [hep-ph].

[56] H. Sun, Y. J. Zhou and H. S. Hou, arXiv:1408.1218 [hep-ph].

[57] S. Fichet, G. von Gersdorff, O. Kepka, B. Lenzi, C. Royon and M. Saimpert, Phys. Rev. D **89**, 114004 (2014) [arXiv:1312.5153 [hep-ph]].

[58] S. Fichet and G. von Gersdorff, JHEP **1403**, 102 (2014) [arXiv:1311.6815 [hep-ph]].

[59] N. Arkani-Hamed, S. Dimopoulos and G. R. Dvali, Phys. Lett. B **429**, 263 (1998) [hep-ph/9803315].

[60] N. Arkani-Hamed, S. Dimopoulos and G. R. Dvali, Phys. Rev. D **59**, 086004 (1999) [hep-ph/9807344].

[61] I. Antoniadis, N. Arkani-Hamed, S. Dimopoulos and G. R. Dvali, Phys. Lett. B **436**, 257 (1998) [hep-ph/9804398].

[62] L. Randall and R. Sundrum, Phys. Rev. Lett. **83**, 3370 (1999) [hep-ph/9905221].

[63] G. F. Giudice, R. Rattazzi and J. D. Wells, Nucl. Phys. B **544**, 3 (1999) [hep-ph/9811291].

[64] T. Han, J. D. Lykken and R. -J. Zhang, Phys. Rev. D **59**, 105006 (1999) [hep-ph/9811350].

[65] H. Davoudiasl, J. L. Hewett and T. G. Rizzo, Phys. Rev. Lett. **84**, 2080 (2000) [hep-ph/9909255].

[66] A. D. Martin, W. J. Stirling, R. S. Thorne and G. Watt, Eur. Phys. J. C **63**, 189 (2009) [arXiv:0901.0002 [hep-ph]].

[67] C. Royon (RP220 Collaboration), arXiv:0706.1796.

[68] V. Avati and K. Osterberg, Report No. CERN-TOTEM-NOTE-2005-002, 2006.

[69] B. C. Allanach, K. Odagiri, M. J. Palmer, M. A. Parker, A. Sabetfakhri and B. R. Webber, JHEP **0212**, 039 (2002) [hep-ph/0211205].

[70] ATLAS Collaboration, Report No. ATLAS-CONF-2012-147.

[71] CMS Collaboration, Report No. CMS-PAS-EXO-12-027.

[72] CMS Collaboration, Report No. CMS-PAS-EXO-12-031.

[73] S. Chatrchyan *et al.* [CMS Collaboration], Phys. Lett. B **714**, 158 (2012) [arXiv:1206.1849 [hep-ex]].

[74] G. Aad *et al.* [ATLAS Collaboration], JHEP **1211**, 138 (2012) [arXiv:1209.2535 [hep-ex]].

[75] G. Aad *et al.* [ATLAS Collaboration], New J. Phys. **15**, 043007 (2013) [arXiv:1210.8389 [hep-ex]].

[76] G. Aad *et al.* [ATLAS Collaboration], Phys. Rev. D **87**, 015010 (2013) [arXiv:1211.1150 [hep-ex]].

[77] M. Marionneau [on behalf of the ATLAS and CMS Collaboration], arXiv:1305.3169 [hep-ex].

[78] G. Aad *et al.* [ATLAS Collaboration], arXiv:1407.2410 [hep-ex].

[79] V. Khachatryan *et al.* [CMS Collaboration], arXiv:1408.3583 [hep-ex].

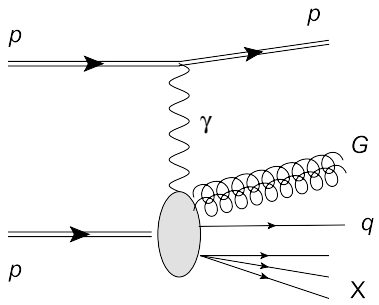

FIG. 1: The photoproduction process $pp \to p\gamma p \to pGqX$.

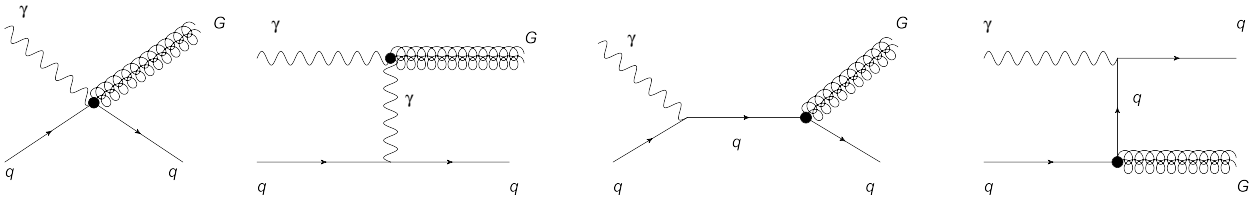

FIG. 2: Tree-level Feynman diagrams for the subprocess $\gamma q \to Gq$ ($q = u, d, c, s, b, \bar{u}, \bar{d}, \bar{c}, \bar{s}, \bar{b}$).

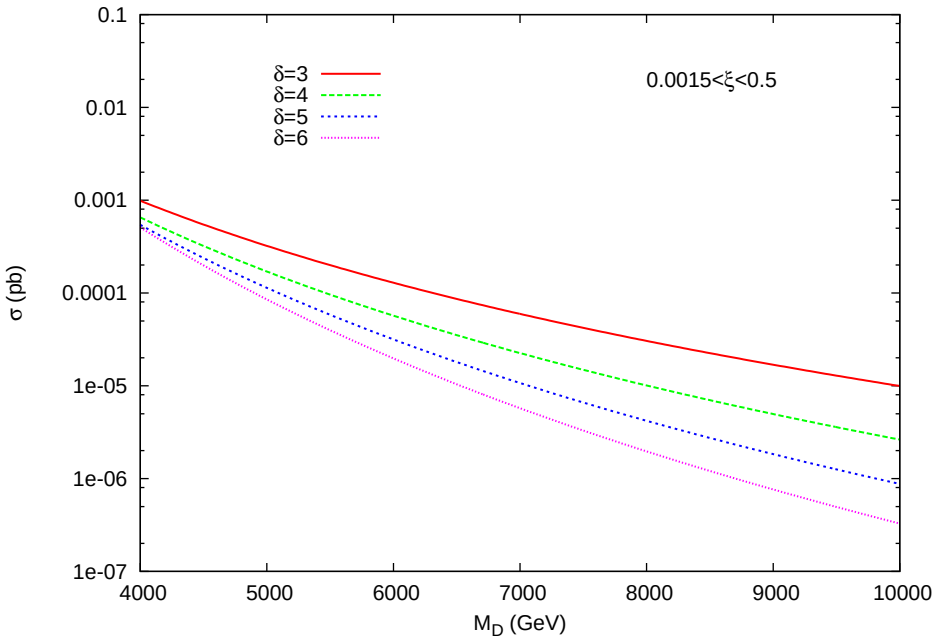

FIG. 3: The total cross section of the process $pp \to p\gamma p \to pGqX$ as a function of the fundamental scale M_D for various number of extra dimensions δ. The forward detector acceptance is chosen to be $0.0015 < \xi < 0.5$.

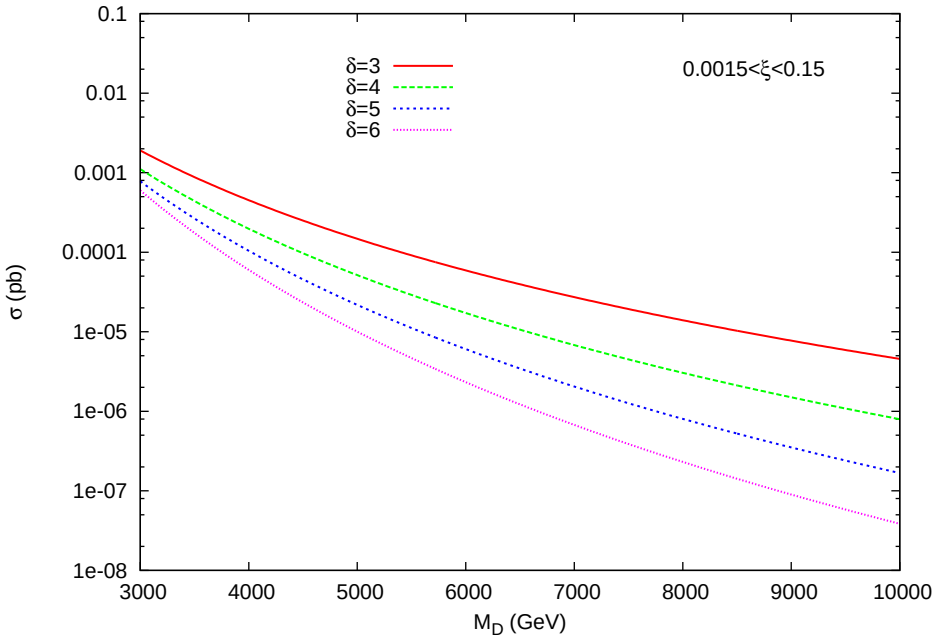

FIG. 4: The total cross section of the process $pp \to p\gamma p \to pGqX$ as a function of the fundamental scale M_D for various number of extra dimensions δ. The forward detector acceptance is chosen to be $0.0015 < \xi < 0.15$.

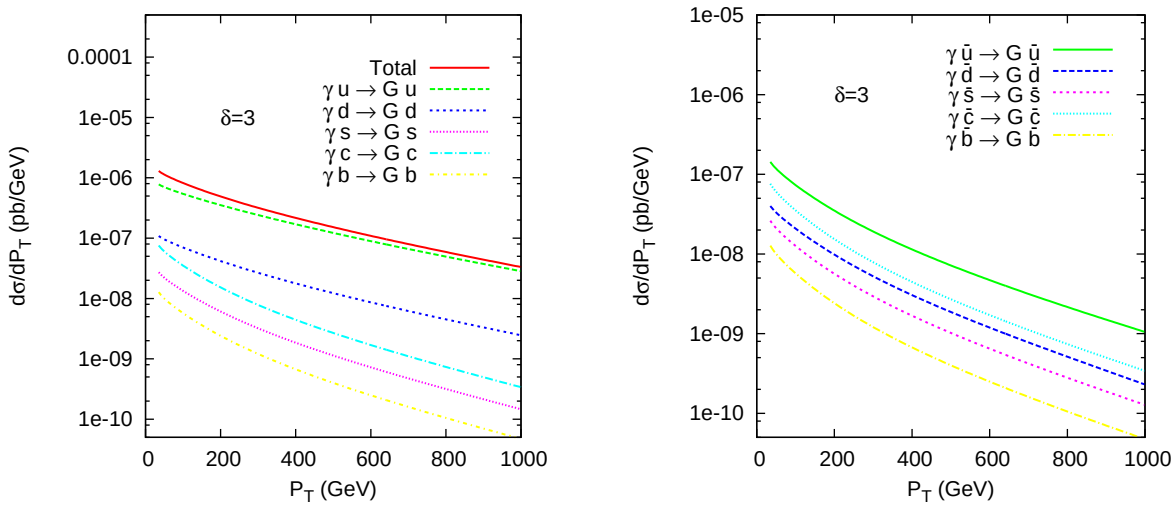

FIG. 5: The differential cross section of the process $pp \to p\gamma p \to pGqX$ as a function of the transverse momentum of the KK tower. The number of extra dimensions is chosen to be $\delta = 3$ and $M_D = 5$ TeV. In the left panel we present total cross section (solid line) which represents the sum of all contributions from subprocesses in (1) and cross sections including individual contributions from each subprocess with quarks. In the right panel we present similar plots but for subprocesses with antiquarks.

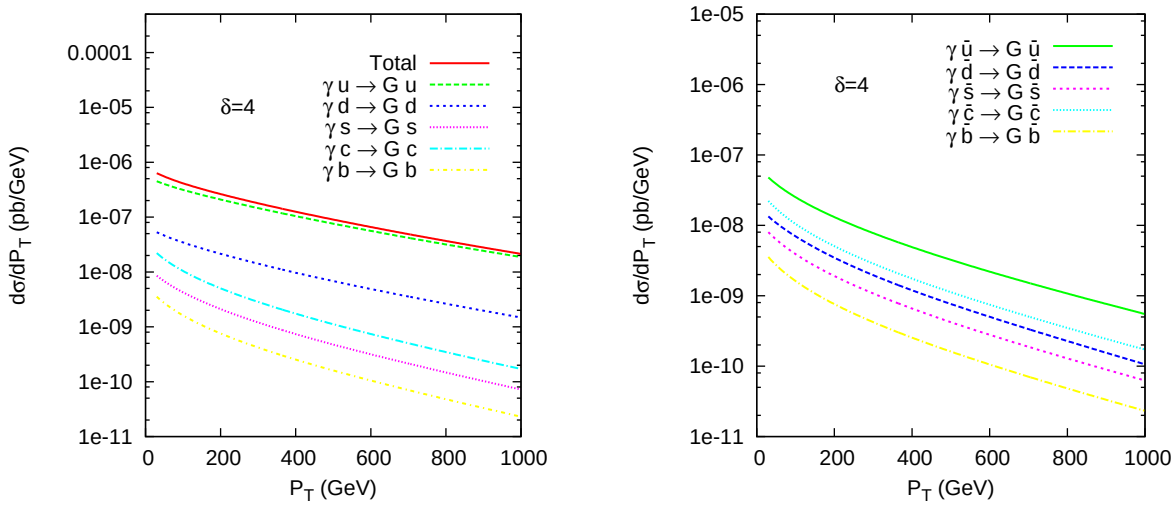

FIG. 6: The same as figure 5 but for $\delta = 4$.

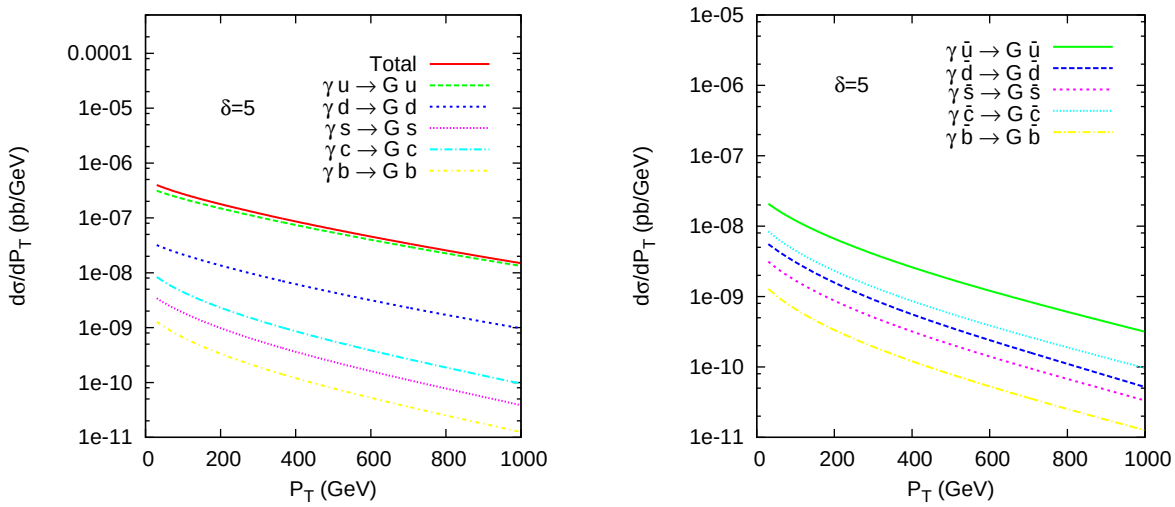

FIG. 7: The same as figure 5 but for $\delta = 5$.

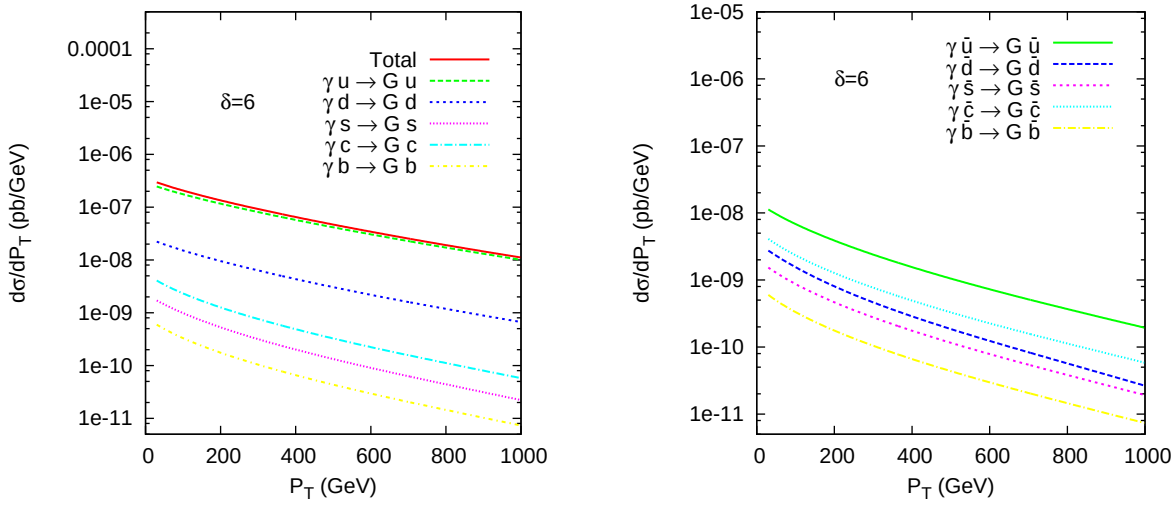

FIG. 8: The same as figure 5 but for $\delta = 6$.

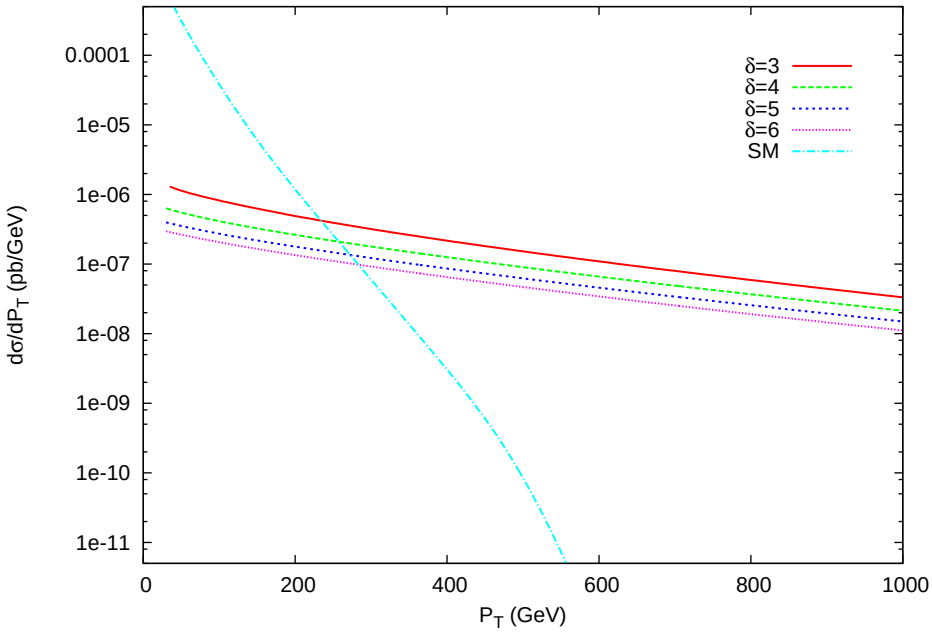

FIG. 9: The missing transverse momentum dependence of the cross section for the process $pp \to p\gamma p \to pGqX$ and Standard Model (SM) background in the center-of-momentum frame of the proton-proton system. VFD acceptance is taken to be $0.0015 < \xi < 0.5$ and M_D=5 TeV.

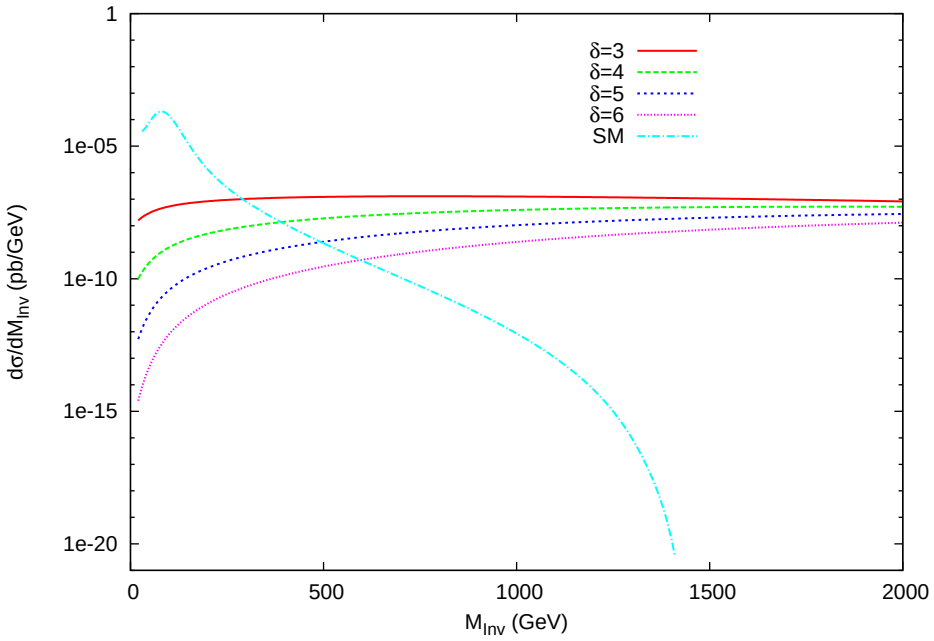

FIG. 10: The missing invariant mass dependence of the cross section for the process $pp \to p\gamma p \to pGqX$ and Standard Model (SM) background in the center-of-momentum frame of the proton-proton system. VFD acceptance is taken to be $0.0015 < \xi < 0.5$ and M_D=5 TeV.

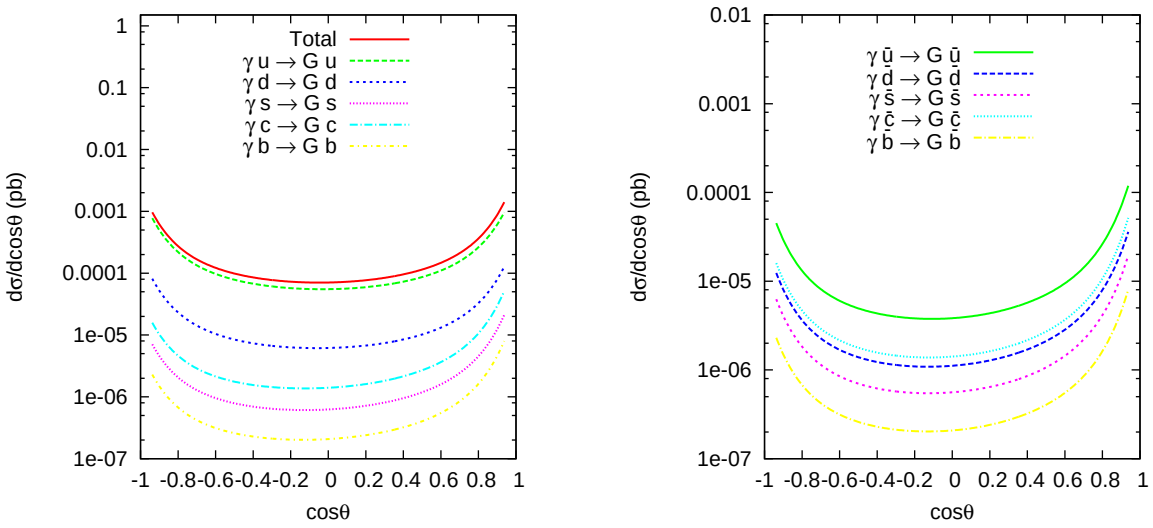

FIG. 11: The angular distribution of the graviton in the center-of-momentum frame of the proton-proton system. θ is the angle between the outgoing graviton and the incoming photon emitting intact proton. RS model parameters are chosen to be $\beta = 0.05$ and $m_G = 1$ TeV. In the left panel we present total cross section (solid line) which represents the sum of all contributions from subprocesses in (1) and cross sections including individual contributions from each subprocess with quarks. In the right panel we present similar plots but for subprocesses with antiquarks.

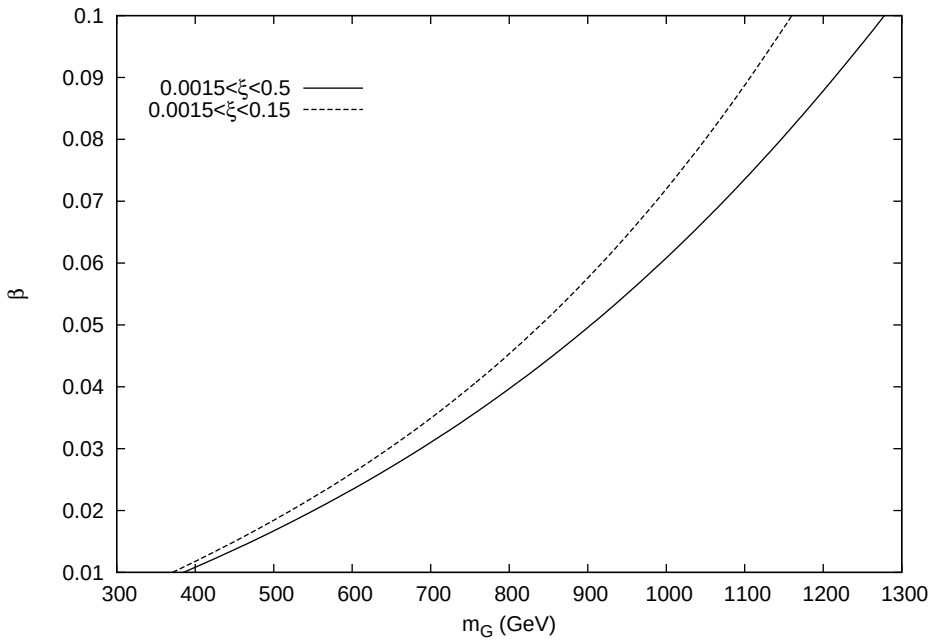

FIG. 12: The 95% C.L. limits in the RS parameter space for an integrated luminosity of 200 fb^{-1} The excluded regions are defined by the area above the curves. $G \to \gamma\gamma, e\bar{e}, \mu\bar{\mu}$ decay channels with a total branching ratio of 8% is considered.

TABLE I: The 95% C.L. bounds on M_D for various integrated LHC luminosities and forward detector acceptance of $0.0015 < \xi < 0.5$. Bounds are given in units of GeV.

Luminosity	$\delta = 3$	$\delta = 4$	$\delta = 5$	$\delta = 6$
$30 fb^{-1}$	5314	4714	4486	4400
$50 fb^{-1}$	5886	5143	4829	4686
$100 fb^{-1}$	6743	5771	5343	5114
$200 fb^{-1}$	7771	6514	5886	5571

TABLE II: The 95% C.L. bounds on M_D for various integrated LHC luminosities and forward detector acceptance of $0.0015 < \xi < 0.15$. Bounds are given in units of GeV.

Luminosity	$\delta = 3$	$\delta = 4$	$\delta = 5$	$\delta = 6$
$30 fb^{-1}$	4560	4112	3552	3356
$50 fb^{-1}$	5028	4224	3804	3608
$100 fb^{-1}$	5784	4748	4224	3916
$200 fb^{-1}$	6636	5336	4692	4280

TABLE III: The 95% C.L. bounds on M_D for various integrated LHC luminosities and forward detector acceptance of $0.0015 < \xi < 0.5$. Bounds are given in units of GeV. We impose a cut of $M_{Inv} > 600$ GeV on the missing invariant mass.

Luminosity	$\delta = 3$	$\delta = 4$	$\delta = 5$	$\delta = 6$
$30 fb^{-1}$	5111	4695	4472	4389
$50 fb^{-1}$	5695	5112	4806	4670
$100 fb^{-1}$	6500	5722	5333	5110
$200 fb^{-1}$	7472	6444	5860	5556

TABLE IV: The 95% C.L. bounds on M_D for various integrated LHC luminosities and forward detector acceptance of $0.0015 < \xi < 0.15$. Bounds are given in units of GeV. We impose a cut of $M_{Inv} > 600$ GeV on the missing invariant mass.

Luminosity	$\delta = 3$	$\delta = 4$	$\delta = 5$	$\delta = 6$
$30 fb^{-1}$	4250	3833	3540	3351
$50 fb^{-1}$	4722	4166	3790	3598
$100 fb^{-1}$	5416	4667	4187	3900
$200 fb^{-1}$	6222	5220	4639	4250